J Mater Sci (2021) 56:11866–11880

Electronic materials

Electrodeposition of cuprous oxide on a porous copper framework for an improved photoelectrochemical performance

Mario Kurniawan[1,*], Michael Stich[1], Mayra Marimon[1], Magali Camargo[1,3], Ralf Peipmann[1], Thomas Hannappel[2], and Andreas Bund[1]

[1] *Electrochemistry and Electroplating Group, Technische Universität Ilmenau, Gustav-Kirchhoff-Straße 6, 98693 Ilmenau, Germany*
[2] *Fundamentals of Energy Materials Group, Technische Universität Ilmenau, Gustav-Kirchhoff-Straße 5, 98693 Ilmenau, Germany*
[3] *Departamento de Ciencias, Instituto de Corrosión Y Protección, Pontificia Universidad Católica del Perú, Sección QuímicaAv. Universitaria 1801, Lima 32, Peru*

Received: 7 December 2020
Accepted: 29 March 2021
Published online: 9 April 2021

ABSTRACT

Photoelectrochemical (PEC) water splitting can be an efficient and economically feasible alternative for hydrogen production if easily processed photoelectrodes made of inexpensive and abundant materials are employed. Here, we present the preparation of porous Cu_2O photocathodes with good PEC performance using solely inexpensive electrodeposition methods. Firstly, porous Cu structures with delicate pore networks were deposited on flat Cu substrates employing hydrogen-bubble-assisted Cu deposition. In a second electrodeposition step, the porous Cu structures were mechanically reinforced and subsequently detached from the substrates to obtain free-standing porous frameworks. In a third and final step, photoactive Cu_2O films were electrodeposited. The PEC water splitting performance in 0.5 M Na_2SO_4 (pH ~6) shows that these photocathodes have photocurrents of up to -2.25 mA cm^{-2} at 0 V versus RHE while maintaining a low dark current. In contrast, the Cu_2O deposited on a flat Cu sample showed photocurrents only up to -1.25 mA cm^{-2}. This performance increase results from the significantly higher reactive surface area while maintaining a thin and homogeneous Cu_2O layer with small grain sizes and therefore higher hole concentrations as determined by Mott-Schottky analysis. The free-standing porous Cu_2O samples show a direct optical transmittance of 23% (λ = 400–800 nm) and can therefore be used in tandem structures with a photoanode in full PEC cells.

Handling Editor: Kyle Brinkman.

Address correspondence to E-mail: mario.kurniawan@tu-ilmenau.de

https://doi.org/10.1007/s10853-021-06058-y

GRAPHICAL ABSTRACT

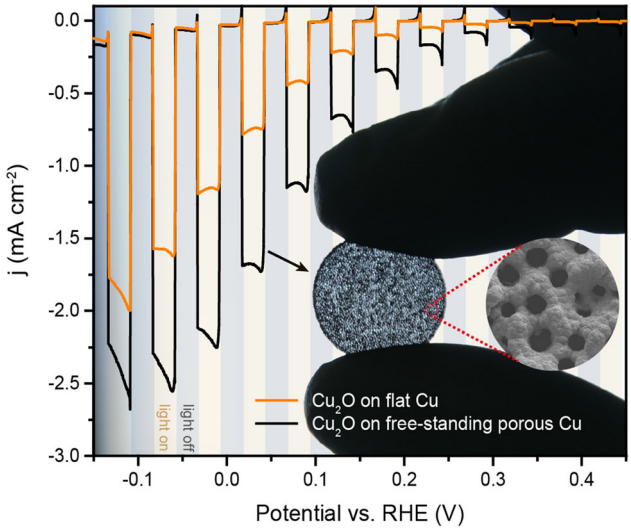

Introduction

Hydrogen is considered as a clean and sustainable energy carrier for the future but is, for economic reasons, currently mainly produced by steam reforming of fossil fuels [1]. A promising method to produce hydrogen from renewable sources is photoelectrochemical (PEC) water splitting [2]. It utilizes direct solar irradiation on photoelectrodes to split water molecules into H_2 and O_2. These photoelectrodes are usually semiconductors with adequate bandgaps and band positions [3, 4].

To make PEC water splitting a competitive and large-scale industrial process, the development of suitable photoelectrodes with high solar-to-hydrogen efficiencies and low costs is required. The semiconductor cuprous oxide (Cu_2O) has been shown to fulfill these criteria and is considered a promising candidate, which can be easily produced by inexpensive electrochemical [5–7] or thermal annealing [8] methods. Cu_2O is a p-type semiconductor which has suitable band positions for PEC water splitting with the conduction band located 0.7 V more negative than the hydrogen evolution reaction (HER) potential [9] and a direct bandgap of ~2.0–2.3 eV, depending on the fabrication process [10–13]. However, the bare Cu_2O has limited chemical stability in the presence of hydrogen evolution (Cu_2O reduces to Cu metal at 0.46 V vs. RHE [14, 15]) and thus is usually coated by thin (< 50 nm) and homogeneous protective layers. Various materials (e.g., TiO_2, ZnO, Al_2O_3, graphite, graphitic carbon nitride, etc.) and methods are available for this purpose and have extensively been researched [16–21]. Additionally, those layers are often modified with electrocatalysts like Pt [14] or Ru [22]. These modifications increase the chemical stability and photocurrent of the Cu_2O electrode, but since so many different materials and processes are used in literature, they make a fair comparison of the underlying Cu_2O performance very difficult. In this paper, we focus only on the bare Cu_2O performance as photocathodes so that we can compare our results better to other publications.

One approach to improve the overall performance for the PEC water splitting of a Cu_2O photoelectrode is by modifying its morphology. An enhancement of the surface area will expose more active sites for the photoelectrochemical reaction and smart nanostructuring can help to overcome one of the Cu_2O intrinsic limitations which is its mismatch between electron diffusion length (typically 20–100 nm) and light absorption depth about 10 µm [23, 24]. On a flat

electrode, a thin Cu_2O layer would be desired to drive enough electrons to the surface, but a thick layer would be necessary to absorb enough photons. However, by modifying the surface morphology in a way that the thin Cu_2O layer is aligned at a more beneficial angle toward the incoming light or the photon pathway, the absorption inside the Cu_2O layer can be increased significantly while still maintaining a small electron diffusion length to the electrolyte. This can practically be achieved by using vertically aligned Cu_2O nanowires or, as seen in the approach pursued in this work, by Cu_2O coated pore walls. The Cu_2O nanowire structure can be synthesized by either using an anodized aluminum oxide template [25], or thermal annealing [22, 26, 27]. However, these methods can face some other limitations such as inhomogeneous Cu_2O coating on a metal substrate. In turn, the overall PEC water splitting performance can be degraded. In contrast, a Cu_2O film prepared by an electrochemical deposition method, which is an inexpensive and scalable synthesis process, shows more reliable performance and can be implemented on rough or 3D substrates with easily tunable layer thickness by adjusting the deposition parameters such as deposition time and current density or applied potential [28]. A report by Luo et al. [22] shows that Cu_2O nanowires synthesized by using wet chemistry and thermal annealing have poor performance due to the exposed underlying metallic Cu. This was overcome by electrodepositing a thin layer of Cu_2O on the existing Cu_2O nanowire photocathode which improves the PEC water splitting performance significantly.

In recent years, electrochemically deposited 3D porous metal structures have shown promising potential to be utilized as electrode materials with large surface areas and high electronic conductivities for applications in fuel cells [29], batteries [30], electrocatalysts [31], and sensors [32]. The synthesis procedure involves the evolution of hydrogen bubbles, which act as dynamic soft templates during the electrodeposition process and create pores in the deposited metal layer. The pore walls of such metal deposits often grow in ramified dendritic structures [33] which increase the surface area of the deposited layers, but on the other hand, reduce their mechanical stability and adhesion, and thus limit their application as substrate materials.

The combination of ramified porous structures and Cu_2O semiconductors has been reported by Ma et al. [8]. The ramified porous Cu underwent a thermal annealing process in a low oxygen atmosphere to oxidize the Cu to Cu_2O which was then used for the PEC water splitting. The current density was reported to reach ~ -2.25 mA cm^{-2} at 0 V versus RHE. However, a relatively high dark current of ~ -1 mA cm^{-2} was observed which according to Ma et al. is possibly due to electrochemical reduction of Cu_2O to Cu, and electrochemical reduction of adsorbed O_2. Besides this approach, to the best of our knowledge, the electrodeposition of Cu_2O on such porous structures has not been reported. Our approach involves producing highly porous, but mechanically stable Cu structures and coating them with a homogeneous Cu_2O film by using only inexpensive electrodeposition methods.

Experimental details

Electrodeposition of dendritic porous Cu

The porous Cu structures were electrodeposited galvanostatically using a potentiostat (Bio-Logic science instruments SP-240 with a ± 4 A booster kit) on a flat Cu substrate at current densities between -0.075 A cm^{-2} and -2.25 A cm^{-2} (Fig. 1). Prior to the electrodeposition procedure, the flat Cu substrate was electropolished in 30 vol. % H_3PO_4 for 1 min at 2 V versus Cu to smoothen the surface (root-mean-square roughness, $R_q = \sim 3$ nm, see Fig. S1). The electrodeposition process was done in a three-electrode configuration with the flat Cu as the working electrode, Pt foil as a counter electrode, and Ag/AgCl in saturated KCl as a reference electrode. An aqueous electrolyte consisting of 0.2 M $CuSO_4$ (Fluka) as Cu source and 1 M H_2SO_4 (Chemsolute) was used. This acidic bath (pH ~ 0) will prevent the formation of oxides on the surface and generate copious amounts of hydrogen for the formation of the porous Cu structure. The flat Cu with an exposed surface area of 1 cm^2 was placed at the bottom of the cell in a horizontal position which allowed a better release of the hydrogen bubbles during the electrodeposition process. The deposition time was varied between 40 and 400 s depending on the applied current density. During the electrodeposition process, two main cathodic reactions occur in parallel (Eqs. 1 and 2). The hydrogen bubbles disrupt the growth of the Cu layer, creating a porous structure with a dendritic wall.

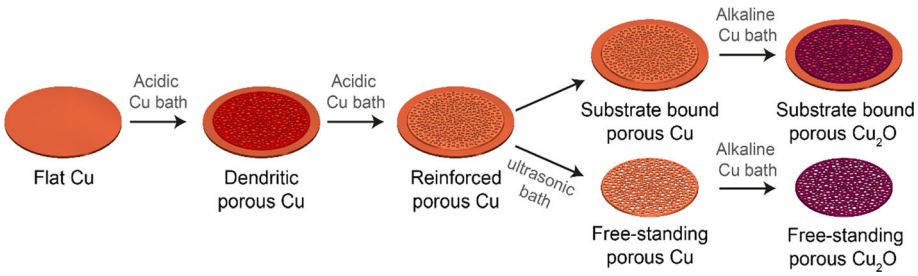

Figure 1 Schematic representation of the electrochemical preparation process of the Cu_2O photocathodes.

$$Cu^{2+} + 2e^- \rightarrow Cu \quad (1)$$

$$2H^+ + 2e^- \rightarrow H_2 \quad (2)$$

Reinforcement process of the dendritic porous Cu

A second Cu deposition was carried out, using the same plating bath with a lower current density of -20 mA cm^{-2} to reinforce the dendritic structures. Prior to the reinforcement process, the cell was shaken a few times to release trapped H_2 bubbles from the pores. The electrodeposition time was varied between 5 and 120 min to evaluate the reinforcement of the dendritic porous Cu.

Lift-off process to produce free-standing porous Cu

Some of the reinforced porous Cu samples were placed in an ultrasonic bath (35 kHz/160 W, Bandelin Sonorex Super RK 510 H) for 5 min. In this process, the ultrasonic vibrations destroy the loosely adhering dendrites. The process was repeated at least 3 times to ensure that all the remaining dendrites were removed completely. Since especially the interface region between the flat Cu substrate and the porous Cu could not be reinforced and remained dendritic, it was possible to peel off the porous Cu layer from the substrate, which resulted in a stable free-standing porous Cu framework.

Electrodeposition of a Cu_2O film

In the next step, the free-standing porous Cu samples and the substrate-bound porous Cu samples were coated with a photoactive Cu_2O film by using the potentiostatic electrodeposition method (Fig. 1). Before that, the samples were etched in 0.1 M H_2SO_4 for 20 s to remove native oxide. Then, the samples were placed in an electrolyte consisting of 0.2 M $CuSO_4$, 1 M $Na_3C_6H_5O_7$ (trisodium citrate, Sigma-Aldrich) as a complexing agent. The pH of this bath was adjusted to ~12 with 6 M NaOH (Carl Roth). The trisodium citrate and the Cu ions will react and form copper(II)–citrate complexes [34, 35] in the electrolyte. This will prevent precipitation of the Cu ions as $Cu(OH)_2$ in an alkaline solution which is needed to ensure a stable formation of the Cu_2O film [36]. In addition, the use of trisodium citrate will help to prevent further oxidation of the Cu_2O film and improve its overall PEC performance as reported by Cao et al. [37]. The cyclic voltammogram (see Fig. S2) shows a reduction peak of Cu_2O at ~ −0.4 V vs. Ag/AgCl (sat. KCl). Therefore, the experiment was carried out using the same electrode configuration as for the previous electrodepositions with an applied voltage of −0.4 V vs Ag/AgCl (sat. KCl). The reduction process to Cu_2O under these conditions is shown in Eq. (3) [38]. The electrolyte was kept at 60 °C using a thermostat and magnetically stirred at 400 rpm. The electrodeposition processes were conducted for 5, 20, and 60 min. Cu_2O is stable at room temperature and dry environment. Further oxidation to CuO occurs above 300 °C [39, 40]. All samples were used directly after preparation.

$$2Cu^{2+}_{(incomplex)} + 2OH^- + 2e^- \rightarrow Cu_2O + H_2O \quad (3)$$

Structural and mechanical characterization

The surface morphologies of the porous substrates and the Cu_2O film were investigated using field-emission scanning electron microscopy (FESEM, Hitachi S-4800). The crystalline structure was characterized by Bragg–Brentano X-ray diffraction (XRD, Siemens/Bruker D5000) using Cu–Kα radiation at 40 kV and 40 mA with a 2θ scan range from 20° to 90° at a scan rate of 0.02° s^{-1}. The thickness of the dendritic porous Cu was investigated using a profilometer (Veeco Dektak 150) with a stylus diameter of 10 µm, an applied mass of 3 mg, and a

resolution of 0.2 μm s^{-1}. A leveling procedure was done using the Dektak software to remove the tilt.

An electrode for PEC water splitting must have sufficient mechanical stability to endure mechanical stresses under operation, e.g., caused by hydrogen evolution. To test the mechanical stability of the porous and reinforced Cu samples, a strong hydrogen evolution was conducted at −100 mA for 2 min in 0.5 M Na_2SO_4. The mass loss during this procedure was measured by an analytical balance (Sartorius AG, BP301S).

Photoelectrochemical measurement

The PEC cell consists of a rectangular PMMA container for ~40 ml of electrolyte. One side of the container holds and electrically contacts the sample. At the opposing side, a 5 mm thick PMMA window allows for the illumination of the sample with a 150 W solar simulator (LOT-QuantumDesign LS0108/15G) with an AM 1.5 filter. The beam intensity of the solar simulator was adjusted using a reference solar cell so that the light intensity at the position of the sample reached 100 mW cm^{-2}. The current densities were recorded with a Biologic potentiostat SP-240 using linear sweep voltammetry (LSV) in a three-electrode configuration under chopped light illumination (5 s light on and 5 s light off) from the solar simulator. The free-standing porous Cu_2O sample was pinned onto a gold-plated brass coin. This provides good contact and exposes only one side of the porous Cu_2O sample to the electrolyte for a better comparison with the substrate-bound samples. The geometric contact area of the samples with the electrolyte was 1 cm^2.

The PEC measurements were carried out in an aqueous electrolyte of 0.5 M Na_2SO_4 (Carl Roth) with pH ~6 from −0.1 to −0.7 V vs. Ag/AgCl (sat. KCl) and a scan rate of 5 mV s^{-1}. The cell was purged with argon for 15 min before the PEC measurements. All the potentials for the PEC measurement discussed below were converted from potential vs. Ag/AgCl (sat. KCl) to the reversible hydrogen electrode (RHE) using Eq. (4) where $\mathring{E}_{Ag/AgCl\ (sat.\ KCl)}$ is the standard potential of 0.197 V at 25 °C and $E_{Ag/AgCl\ (sat.\ KCl)}$ is the measured working potential.

$$E_{RHE} = E_{Ag/AgCl\ (sat.\ KCl)} + 0.059pH + E^{\circ}_{Ag/AgCl\ (sat.\ KCl)} \quad (4)$$

This conversion was performed because the potential versus RHE is independent of the pH value and thus simplifies the comparison with other literature data.

Mott-Schottky analysis

At the interface between a semiconductor electrode and an electrolyte, two regions of charge separation are found, the space charge region in the semiconductor and the electrochemical double layer in the electrolyte. The capacitance of the space charge region is usually much smaller than the capacitance of the electrochemical double layer and since they are connected in series, the capacitance of the space charge region determines the overall capacitance. Experimentally this capacitance can be measured by electrochemical impedance spectroscopy (EIS), where a small sinusoidal voltage (15 mV) with varying frequency (between 63 and 30 kHz) is applied to the working electrode. The experimental setup consists of the three-electrode configuration and electrolyte (0.5 M Na_2SO_4) used for the previous PEC measurement including purge with argon gas for 15 min.

To determine the space charge capacitance at different potentials, the potential was scanned from −0.1 to 0.15 V vs. Ag/AgCl (sat. KCl) in steps of 6 mV using the staircase potentio electrochemical impedance spectroscopy (SPEIS) method. By plotting the reciprocal of the square of capacitance (C^{-2}) against the potential, one obtains a Mott-Schottky plot which is generally used to determine characteristic parameters of semiconductors, such as flat-band potential and charge carrier density (acceptors or donors). The semiconductor type can also be determined from the positive (n-type) or negative (p-type) sign of the slope between the charge accumulation plateau and charge depletion plateau seen in the Mott-Schottky plots (Fig. 8). When the applied voltage for a p-type semiconductor is more positive than the flat-band potential, charge accumulation occurs resulting in low C^{-2} values. Vice versa, a more negative potential leads to charge depletion, resulting in high C^{-2} values. The linear part of the curves between the accumulation and depletion plateau was fitted with a linear equation and extrapolated to the intersection with the abscissa. The potential at this value represents the flat-band potential and the slope of the linear equation can be used to estimate the charge carrier density, N_a, according to Eq. (5).

$$\frac{1}{C^2} = \frac{-2}{\varepsilon_r \varepsilon_0 A^2 e N_a}\left(E - E_{fb} - \frac{k_B T}{e}\right) \quad (5)$$

In Eq. (5), C is the space charge capacitance, ε_r is the relative dielectric constant of Cu_2O (7.6) [41], ε_o is vacuum permittivity, A is the surface area of the electrode (roughness factor is included), e is the elementary charge, N_a is the acceptor charge carrier density, E is the applied potential, E_{fb} is the flat band potential, k_B is Boltzmann constant and T is the absolute temperature.

Results and discussion

Dendritic porous Cu template

Important parameters to improve the overall performance of the PEC water splitting are the active area and the surface morphology. Increasing the active area and optimization of the morphology creates more active sites for the photoelectrochemical reactions. By varying the electrodeposition durations (40–400 s) and current densities (−0.075 to −2.25 A cm^{-2}), different morphologies (Fig. 2) could be obtained. The walls of the porous structures are made of small ramified structures as was also reported by Shin et al.[33]. All porous Cu layers were deposited with an average thickness of 200–250 µm for better structural comparison (see Fig. S3).

For low current densities and long deposition times, only a small amount of widely scattered porous structures were obtained. At higher current densities, starting from −0.37 A cm^{-2} with deposition times of 160 s (Fig. 2c) the substrate gets fully covered with porous structures. The formation of these porous structures is strongly influenced by the amount and size of hydrogen bubbles produced on the surface. The hydrogen bubbles act as insulating objects, blocking the active sites for the growth of Cu [42]. The high current densities trigger higher production of hydrogen and increase the detachment rate of the bubbles from the substrate surface which influences the modification of the pore size diameter. At lower current densities, the Cu deposition has a higher current efficiency (see Fig. S4b), due to a decrease in the hydrogen evolution rate and thus reduces the porosity of the samples (Fig. 1a and b). By increasing the current density up to −0.75 A cm^{-2}, the average pore size on the top layer decreases from ~300 µm (Fig. 2a–c) to ~100 µm (Fig. 2d–f). Beyond −0.75 A cm^{-2}, there is no significant difference in the average pore size, but the number of interconnecting pore tunnels as shown in the insets in Fig. 2d–f increases. It can be observed from the insets of Figs. 2 and Fig. 3a that the walls of the porous structures are made of ramified dendrite structures and contain gaps. The formation of these dendritic structures at the pore walls is triggered by

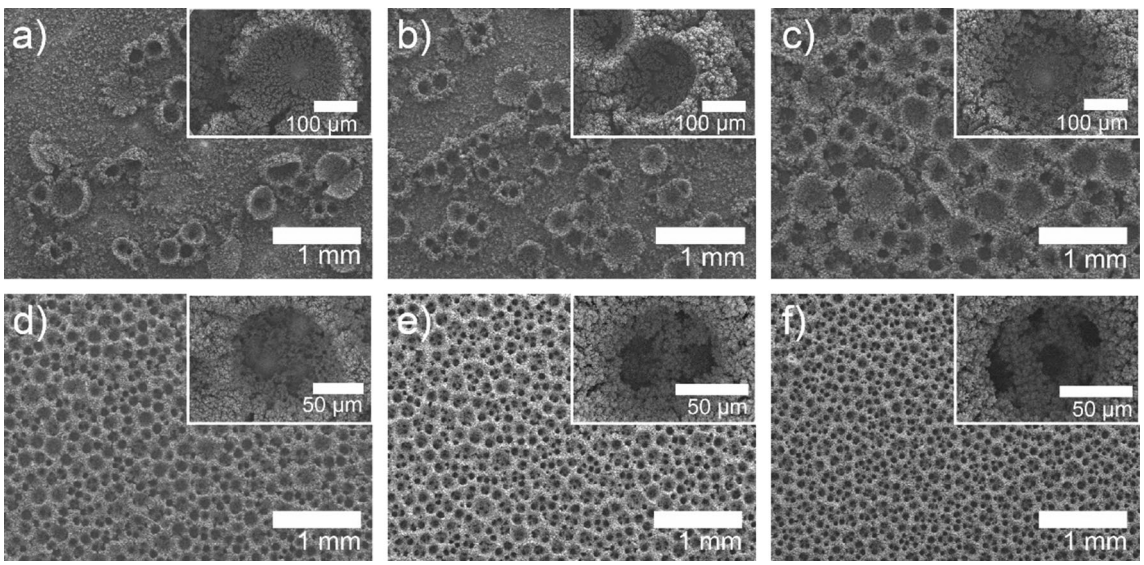

Figure 2 Scanning electron micrographs of the electrodeposited dendritic porous Cu structures on a flat Cu substrate using different current densities and deposition durations: **a** −0.075 A cm^{-2}, 400 s; **b** −0.15 A cm^{-2}, 240 s; **c** −0.37 A cm^{-2}, 160 s; **d** −0.75 A cm^{-2}, 100 s; **e** −1.5 A cm^{-2}, 60 s and **f** −2.25 A cm^{-2}, 40 s. The insets show magnified images of the pores.

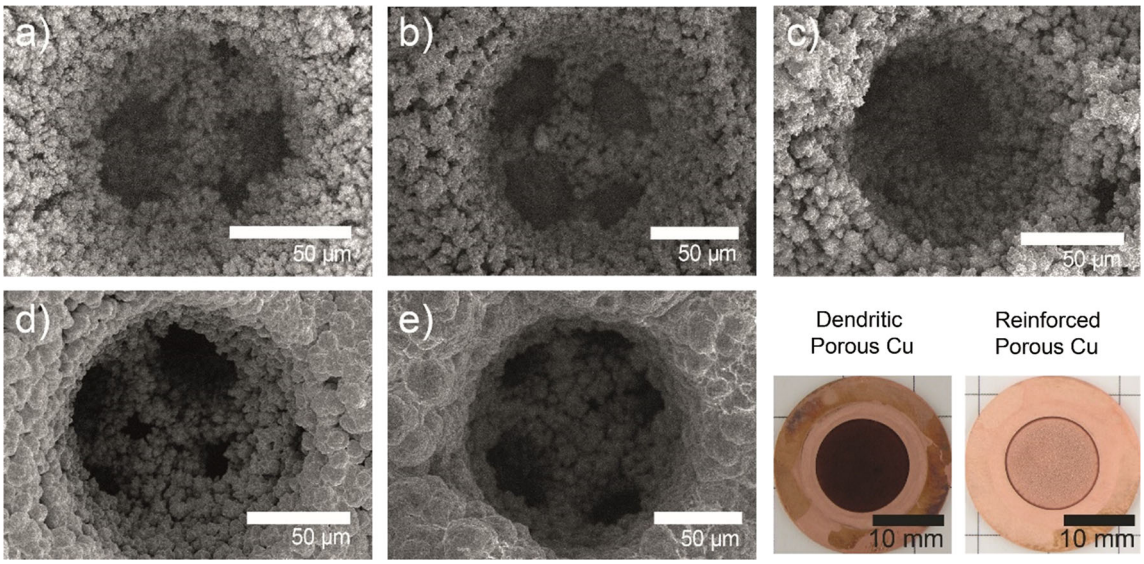

Figure 3 Reinforcement procedure of the dendritic porous Cu (deposited at 1.5 A cm^{-2} for 60 s) with **a** no reinforcement **b** 5 min, **c** 30 min, **d** 60 min and **e** 120 min Cu deposition time at current densities of −20 mA cm^{-2} The two images shown on the right bottom corner are the sample photographs.

surface irregularities such as micro-protrusion which appeared due to preferential deposition of the Cu metal on the active sites. More details on the formation mechanism of these dendritic Cu structures as well as their surface properties have been reported by Wang et al. [43]. Although these dendritic structures increase the surface area tremendously, they are extremely fragile and would be damaged or destroyed in a real PEC water splitting application. Therefore, to investigate the mechanical stability of the dendritic porous Cu during water splitting, the mechanical characterization based on the hydrogen evolution reaction as described in the experimental section was carried out. The mass of the dendritic porous Cu sample (−1.5 A cm^{-2} for 60 s) decreased by ~22% from 21.1 ± 0.1 mg to 16.3 ± 0.1 mg. The dendritic structure disintegrated during the process, and small Cu particles could be observed at the bottom of the cell. This shows that the dendritic porous Cu has poor mechanical stability and will have to be reinforced to be used as a substrate material for the PEC water splitting application.

Free-standing porous Cu

To improve the surface morphology and the mechanical stability of the dendritic porous structures, a second Cu deposition process with a small current density of −20 mA cm^{-2} was carried out on the sample deposited at −1.5 A cm^{-2} for 60 s. This relatively small current density is an important parameter to significantly reduce the hydrogen evolution and enable a homogeneous deposition for a compact Cu layer. Thereby, the gaps in the dendritic morphology of the pore walls (Fig. 3a) are filled with increasing deposition duration as shown in Fig. 3b–e. This transformation, which changes the surface morphology and roughness, also influences the color of the sample as can be seen in the photographs in Fig. 3. Starting from 60 min of the reinforcement process, the structure is more compact and allows its use as a stable substrate for the subsequent Cu_2O deposition (see Fig. S5).

Despite the reinforcement procedure, the bottom part of the reinforced porous Cu is still in its dendritic form (Fig. 4a). Probably the limited transport of the Cu ions through the inner pores near the substrate hinders the deposition process at the bottom region. On the other hand, the weak structural integrity at the bottom region allows the porous Cu layer to be removed easily by ultrasound and form a free-standing framework as shown in Fig. 4b and c. The interconnected pore networks that were observed at the interface between the reinforced porous Cu and the flat Cu substrate, are also absent on the free-standing porous Cu as observed from the top view images in Fig. 4a, and b. It is obvious that the ultrasonic process successfully removed the dendritic

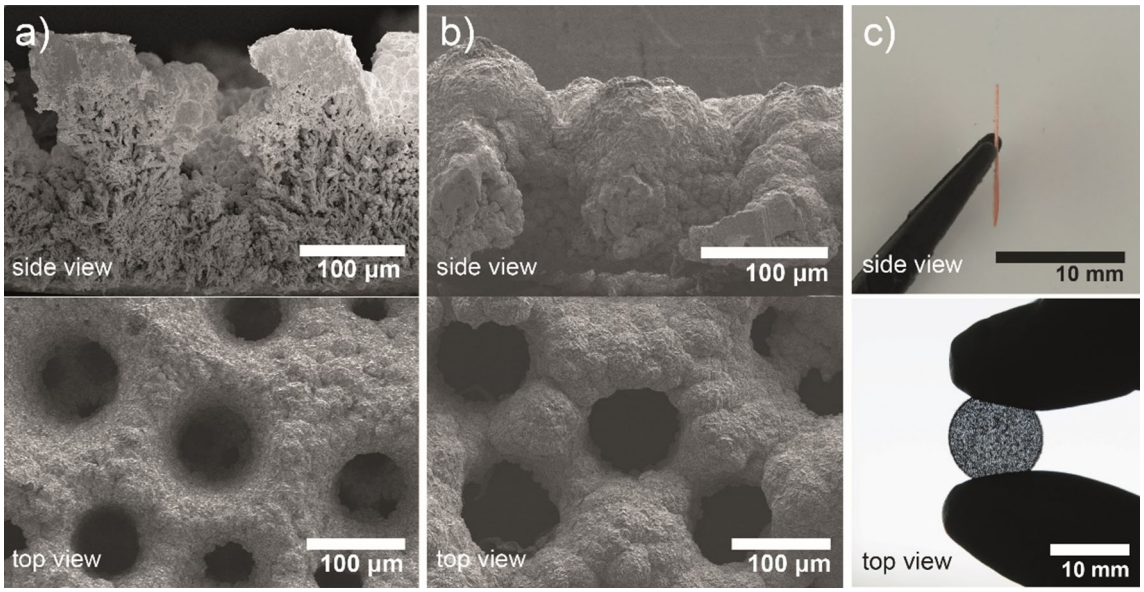

Figure 4 Morphological comparison of **a** substrate-bound and **b** free-standing porous Cu electrodeposited at -1.5 A cm^{-2} for 60 s and reinforced with a second Cu electrodeposition using -20 mA cm^{-2} for 120 min. An ultrasonic bath was used to separate the porous layer from the flat Cu substrate and produce a free-standing porous Cu layer (the top image shows the cross-section of the samples and the bottom part shows the top view). **c** Sample photographs of the free-standing porous Cu.

layer, which consists mostly of these interconnected pore networks, and thereby created single through pores. As mentioned previously, Cu_2O layers coated on those trough pore walls have a beneficial orientation for light absorption, while keeping the short diffusion length of minority charge carriers to the electrolyte. The improvement in mechanical stability via the reinforcement procedure and subsequent lift-off can be demonstrated by the mechanical characterization, which shows no mass loss for these samples after 2 min of strong hydrogen evolution. The average pore diameter of the free-standing porous Cu was estimated from the SEM images to be in the range of 50–100 µm. During the removal process of the dendrites in the ultrasonic bath and the subsequent lift-off from the substrate, the thickness of the porous Cu layer decreased by ~32% (from ~250 µm for the substrate-bound sample to ~170 µm for the free-standing sample).

While pore walls open the possibility to mitigate the mismatch between adsorption and diffusion length, they also allow part of the light to pass through the photoelectrode. Controlling the pore size by adapting the parameters of the Cu electrodeposition (current density, deposition time) enables the tuning of light transmission through the free-standing porous Cu in such a way that a photoanode behind the photocathode could harvest the transmitted light in a full cell configuration or dual photocathode configuration as was reported by Niu et al. [44].

By using ultraviolet–visible (UV–Vis) spectroscopy (Varian Inc., Cary 5000) with a spectral range between 400 and 800 nm, the direct optical transmittance of the sample deposited with an applied current density of -1.5 A cm^{-2} for 60 s and reinforced with -20 mA cm^{-2} for 120 min was measured to be ~23% (see Fig. S6).

Cu_2O film on different porous substrates

The electrodeposition of the photoactive Cu_2O layer on top of porous and solid Cu substrates was done potentiostatically and the measured currents normalized by the geometric surface area (Fig. 5a). The current densities represent the growth rates of the Cu_2O films, assuming 100% faradaic efficiency. For all samples, the deposition on the pristine Cu surface starts with high values of the absolute current densities that decrease over time, as the surface is getting gradually covered with the less conductive Cu_2O layer. However, the dendritic porous Cu and the reinforced substrate-bound samples show similar behavior of the current densities which become almost constant after 15 s. The dendritic porous Cu in

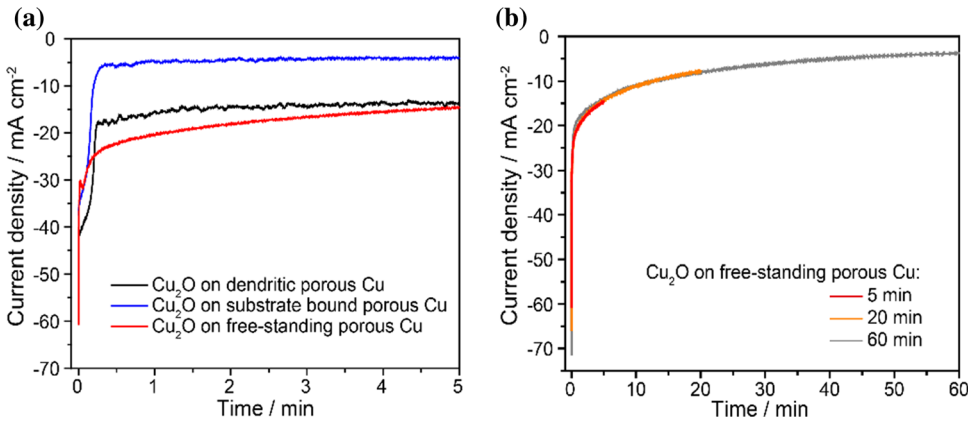

Figure 5 Current transients of **a** Cu_2O film electrodeposited on different substrates for 5 min and **b** Cu_2O film electrodeposited on free-standing porous Cu substrates at different deposition times.

its non-reinforced state has a very large surface area, which leads to current densities in the range of −14 to −18 mA cm^{-2} after 15 s. The reinforced substrate-bound sample, on the other hand, is more compact and has a considerably smaller surface area (Fig. 4) which results in smaller current densities in the range of −6 to −4 mA cm^{-2}. For both the dendritic porous Cu and the substrate-bound porous Cu, the diffusion of the Cu ions through the small-ramified pores and the complex interconnecting pore networks at the interface might be a limiting factor in the deposition process.

The free-standing porous Cu, which is reinforced and separated from the flat Cu substrate, was exposed to the electrolyte from the front side and the backside. This makes the pore surface more accessible and results in even higher deposition currents than the dendritic porous Cu. The chronoamperometric curve of the Cu_2O deposition on free-standing porous Cu (Fig. 5b) shows that the current densities have similar behavior for all samples which indicates good reproducibility for the preparation of the porous substrates. There is a rapid change in the current densities at the initial stage and then the current decreases at a slower rate over a long deposition time scale which is typical behavior for a potentiostatic process.

The grains of the Cu_2O on the free-standing porous Cu substrate grow larger with increasing deposition time (Fig. 6a–c). For a deposition time of 5 min (Fig. 6a), the SEM micrograph shows a thin layer consisting of grains with sizes between 500 and 800 nm. With increasing deposition time, the grain size increased to about 2–4 µm. However, no significant change in the grain size of the 20 min sample and the 60 min sample (Fig. 6b–c) could be observed. This trend can be linked to the current transient of the Cu_2O (Fig. 5b), which shows that the deposition current decreases at a much slower rate after 20 min deposition time due to the gradual increase of the amount of the less conductive Cu_2O. This indicates that the deposition time has a strong influence on the layer morphology and the electro-crystallization process.

Due to the complex morphology of the porous structure, it is challenging to measure the thickness of the Cu_2O layer directly. Therefore, an indirect approach to estimate the layer thickness is taken here. Since a potentiostatic electrodeposition method is used, the upper limit of the achievable thickness can be expected from the electrodeposited Cu_2O layer on the flat Cu substrate which was deposited using the same parameters (electrode configuration, potential bias, temperature, and pH) as for the porous Cu substrate with various deposition times. From the cross-sectional SEM images of the Cu_2O layer on flat Cu (see Fig. S7), the thickness varies between ~500 nm and ~3 µm for the samples with 5 min and 60 min deposition time, respectively.

XRD analysis was used to confirm the identity and the crystal structure of the Cu_2O film. The XRD patterns in Fig. 6d show the comparison of the Cu_2O samples on the free-standing porous Cu with different deposition times. The diffraction peaks matched the XRD pattern of bulk Cu_2O (JCPDS 01-077-0199) with the most intense peaks for the (111) plane, which is a photoactive facet[45], followed by the (200) and (220) planes. The (111), (200), (220), and (311) planes from the porous Cu substrate (JCPDS 01-085-1326) were also present. The sample with 5 min deposition time exhibits five prominent reflections. The peak at 36.4° belongs to the Cu_2O (111) plane and the four

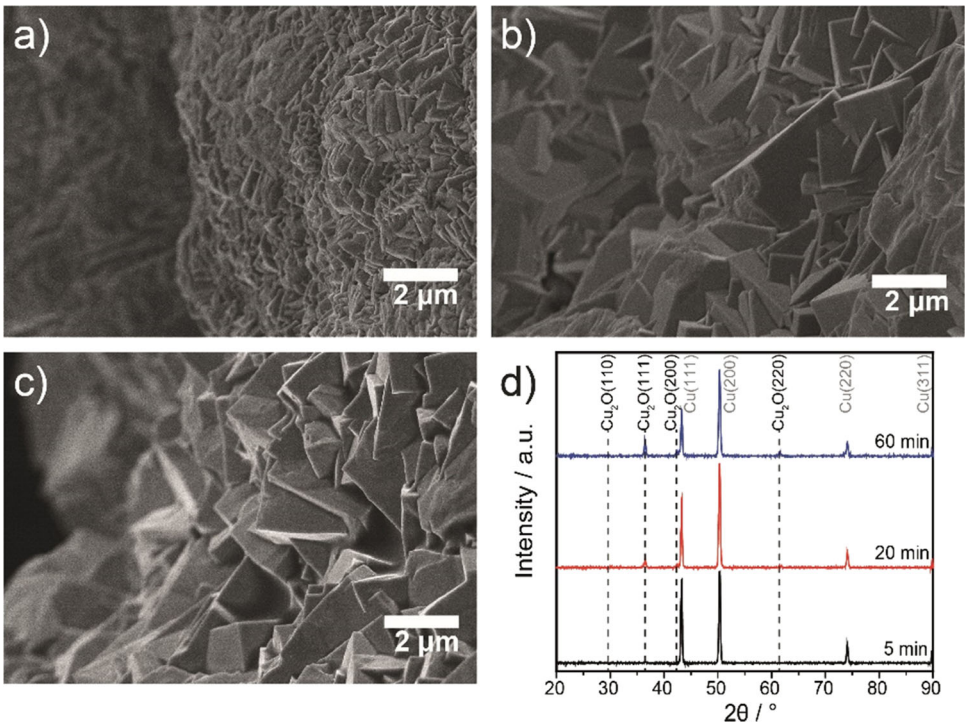

Figure 6 Surface morphology comparison of Cu_2O films electrodeposited potentiostatically at −0.4 V vs. Ag/AgCl (sat. KCl) on the free-standing porous Cu substrate for **a** 5 min, **b** 20 min, and **c** 60 min deposition time in a Cu citrate bath (pH 12) and **d** XRD patterns of those Cu_2O films.

remaining peaks belong to the porous Cu substrate for the (200) and (111) planes. For the 20 min and 60 min samples, there is a significant increase in the intensities of most of the Cu_2O diffraction peaks, especially for the (111) plane while the peak intensity of the porous Cu substrates gradually decreases. The full-width-half-maximum (FWHM) of the Cu_2O (111) plane from the 5 min, 20 min and 60 min samples decrease progressively from 0.44° to 0.41° and finally to 0.35°, respectively. By using the Scherrer equation, crystallite sizes of 22, 24, and 28 nm can be estimated. None of the investigated samples showed reflections belonging to cupric oxide (CuO), confirming the suitability of the electrodeposition method for producing stable Cu_2O layers. The XRD pattern that was obtained using the Bragg–Brentano method is used to provide information regarding the crystal plane that is parallel to a planar surface. The crystal orientation of the Cu_2O influences the crystal facet which is an important factor to improve the performance for the PEC water splitting [45]. In the case of the free-standing porous sample, the Cu_2O was deposited on the top and the inner part of the pore walls. This means that XRD not only probes the parallel crystal planes of the Cu_2O but the perpendicular plane as well (the inner part of the pore wall). As a result, the samples exhibit a powder-like behavior, not because of the intrinsic different crystal plane orientations but due to the special morphology of the porous Cu substrate. As a consequence, it would be rather challenging to determine the texture of the Cu_2O film more quantitatively.

PEC performance of Cu_2O photocathodes

Figure 7 shows the results of LSV measurements with a scan rate of 5 mV s^{-1} under chopped illumination of Cu_2O films deposited on different substrate types as well as layers obtained at different deposition times on free-standing porous Cu frameworks, respectively.

All samples in Fig. 7a were deposited with Cu_2O films at −0.4 V vs. Ag/AgCl (sat. KCl) in an alkaline bath for 5 min. Under illumination, the Cu_2O deposited on the flat Cu substrate shows a photocurrent of ~ -1.25 mA cm^{-2} at 0 V vs. RHE as shown in Fig. 7a. In the dark (light off), the current density of this sample stays constant and close to zero in the potential range between 0.4 and 0 V vs. RHE and then slightly increases to ~ -0.15 mA cm^{-2} at −0.15 V vs. RHE. For the dendritic porous Cu_2O sample, the overall current density increases significantly, but this increase is mostly caused by an undesirably high dark current. In our opinion, there are probably two main reasons why the dark current

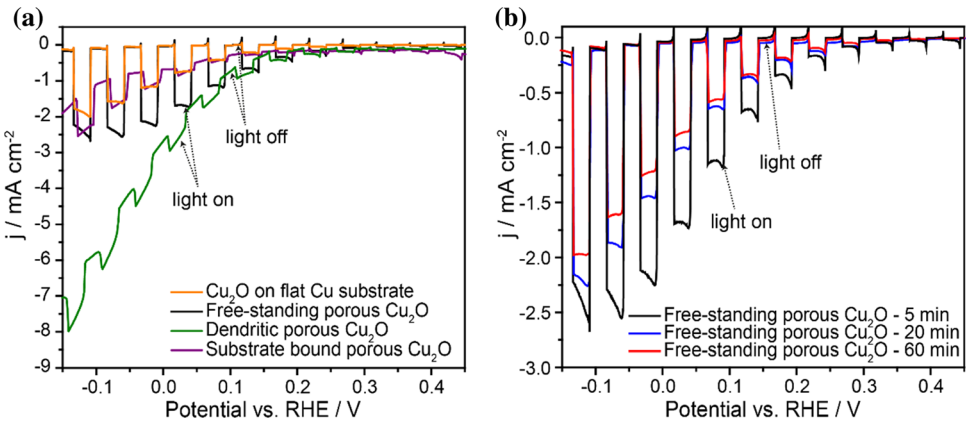

Figure 7 Photoelectrochemical analysis of **a** Cu_2O film deposited for 5 min on different Cu substrates and **b** Cu_2O film deposited on a free-standing porous Cu with different durations using an applied potential of −0.4 V vs. Ag/AgCl (sat. KCl). The measurements were done in 0.5 M Na_2SO_4 (pH ~6) under chopped illumination.

of the dendritic porous Cu_2O sample is higher than that of the flat Cu_2O sample. (1) The surface area of the dendritic porous sample is much higher than the surface area of the flat Cu_2O sample and therefore the electrochemical reduction process of Cu_2O to Cu is accelerated. (2) The deposition of Cu_2O on the dendritic porous Cu is likely to be inhomogeneous and thin Cu_2O layers are expected in the dendrite structures due to transport limitations of the Cu ions into the small pores. The thickness of the Cu_2O layer seems to be related to its reactivity without illumination. Thicker layers of the semiconductor Cu_2O are less prone to reduction due to their increased electrical resistivity and cause a lower dark current (see also Fig. 5b), while the relatively thin Cu_2O layers in the dendritic structures are more reactive. The two reinforced samples in Fig. 7a (free-standing and substrate-bound) show higher photocurrents than the flat sample, but the substrate-bound Cu_2O sample shows a high dark current while the free-standing Cu_2O sample does not. The cause for this is probably again the inhomogeneously coated dendritic Cu, which is still present for the substrate-bound sample (see Fig. 4a). The free-standing sample on the other hand shows a higher photocurrent density of -2.25 mA cm^{-2} at 0 V vs. RHE which is 80% higher than the photocurrent of Cu_2O on flat Cu while still maintaining a very low dark current (see Fig. S8). These promising results, which could not be obtained by the Cu_2O synthesis via thermal oxidation on dendritic porous Cu[8] (photocurrent: -2.25 mA cm^{-2}, dark current: -1 mA cm^{-2}), show that the electrodeposition method can stabilize the Cu_2O reduction when deposited on a suitable, high surface area substrate. The stabilization of Cu_2O reduction and decrease of the dark current is likely to be caused by a high-quality homogeneous Cu_2O layer. Furthermore, our results also show a significant improvement compared to the other bare Cu_2O photocathodes (see Table S1) prepared on Cu substrates with nanowire structures (photocurrent: -2.08 mA cm^{-2}, dark current: -0.3 mA cm^{-2}[46] and photocurrent: -0.5 mA cm^{-2}, dark current: close to zero [47]). However, planar Cu_2O films on Au and FTO substrates show a slightly higher photocurrent probably due to the preferred crystal orientation which has been reported to affect the PEC water splitting performance[45]. The deposition time of the Cu_2O film on the free-standing porous Cu also influences the photocurrent density (Fig. 7b), even though it has only a negligible impact on the bandgaps, which are estimated at ~ 2 eV (see Fig. S9). The short deposition time of 5 min leads to the highest photocurrents, while longer deposition times decrease the photocurrent. To evaluate the influence of Cu_2O deposition time on the chemical stability of the free-standing porous Cu_2O samples, the LSV measurements were repeated three times (see Fig. S10). The photocurrent of the 5 min deposited sample degrades at a much faster rate from -2.25 to -1 mA cm^{-2} at 0 V vs. RHE between the first two sweeps whereas the photocurrent of the 20- and 60-min deposited samples reduces at a much slower rate. This indicates that the PEC degradation is strongly influenced by the layer thickness which demonstrates that the thicker bare Cu_2O layer has

slower photodegradation than the thin and more catalytic Cu_2O film. Further investigation of the free-standing porous Cu_2O for the long-time stability measurement and PEC water splitting efficiency will not be discussed here because it can only be determined after a protective coating is applied to the layer.

Mott-Schottky plots (Fig. 8a–c) were performed at frequencies of 30, 40, 50, and 63 kHz to determine the flat-band potential and charge carrier density of the Cu_2O layers deposited on the free-standing porous Cu samples at various deposition times (5, 20, and 60 min). The data confirm that the Cu_2O semiconductor is of p-type, due to the negative slope between the high plateau and low plateau observed in these graphs. The flat-band potential lies between 0.63 and 0.66 V vs. RHE (Fig. 8d) which is in agreement with the values reported in the literature (~0.65 V vs. RHE) [22] and placed the conduction band position to be more negative than the HER potential. The chronoamperometric curve in Fig. 5b shows reproducible currents for the Cu_2O deposition. This suggests that the surface areas of the underlying free-standing porous Cu frameworks are very similar. The reproducibility of the morphology and the pore sizes of the samples is also supported by the SEM images in Fig. S11. Since the surface area of the free-standing porous Cu does not vary significantly between samples and the thin Cu_2O layer does not have a significant influence, most of the surface area change is probably due to the roughness variation due to the different crystallinity of the Cu_2O film deposited at different durations. The surface roughness of the samples was investigated by AFM (see Fig. S12) using the Nanoscope Analysis software from Bruker. The roughness factor was then extracted from the local surface area increase which was estimated to be 1.17, 1.36, and 1.41 for the samples deposited for 5 min, 20 min, and 60 min, respectively. The charge carrier densities were then calculated by considering the roughness factor to the surface area in Eq. (5) which provides the value between $\sim 2.5 \times 10^{17}$ and $\sim 4.9 \times 10^{18}$ cm^{-3} (Fig. 8e). While the variation in the flat-band potential is minor among the three samples over the investigated range of frequencies, the charge carrier density varies more strongly. Especially for the deposition time of 5 min, an increase in the hole concentration of $\sim 4.9 \times 10^{18}$ cm^{-3} could be observed. This high value might be caused by the

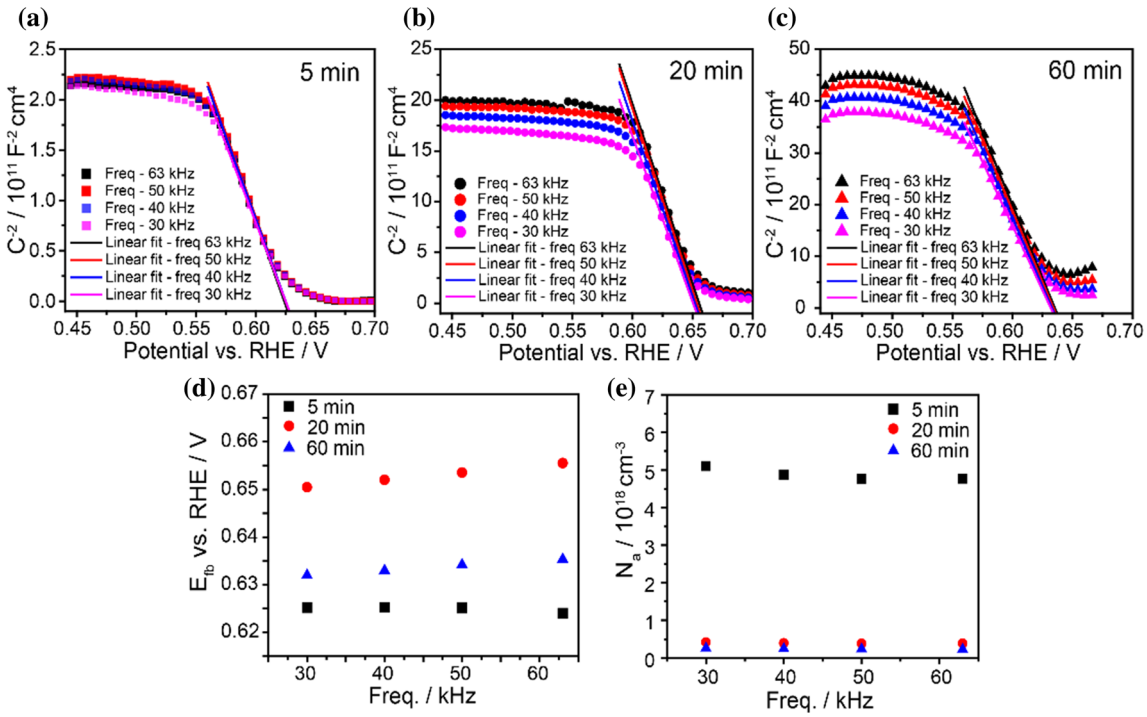

Figure 8 Mott-Schottky plots of deposited Cu_2O films on free-standing porous Cu for **a** 5 min, **b** 20 min and **c** 60 min deposition time at various frequencies in 0.5 M Na_2SO_4 (pH ~6). The flat-band potential E_{fb} and the charge carrier density N_a were plotted against the frequency in (**d**) and (**e**), respectively.

smaller grain size of the Cu_2O crystals as well as the thinner layer thickness which can influence the conductivity of the film and thus contribute to the improvement of the overall PEC water splitting performance as was shown in Fig. 7b. The influence of the various frequencies on the charge carrier density is relatively small which suggests that the chosen frequency range is suitable for a reliable determination of the doping level of this system.

Conclusions

A preparation route has been suggested to produce efficient Cu_2O photoelectrodes using only electrodeposition processes. Hydrogen-evolution-assisted copper electrodeposition was used to create a dendritic porous Cu structure with a high surface area. Higher current densities produced a better distribution of the pores, increased interconnecting pore networks, and reduced the average pore size from ~300 µm to ~100 µm. A second electrodeposition procedure was carried out at a lower current density (-20 mA cm^{-2}) to mechanically reinforce the dendritic porous Cu structures. Subsequently, an ultrasonication process separates the reinforced porous layer from the flat Cu substrate to form a stable free-standing porous Cu framework, which has tubular shaped through pores.

A layer of Cu_2O was electrodeposited in an alkaline copper bath on various porous and flat Cu substrates. The PEC water splitting results revealed that the Cu_2O film deposited on a flat Cu substrate showed a photocurrent density of ~-1.25 mA cm^{-2} at 0 V vs. RHE under 1.5 AM illumination. The best overall results were obtained for the free-standing porous Cu_2O sample, combining a high overall current density (~ -2.25 mA cm^2 at 0 V vs. RHE), which is 80% higher than the Cu_2O on flat Cu substrate, with a low dark current. The special geometry of the free-standing Cu framework allows for Cu_2O coated tubular pore walls, which are preferentially oriented toward the irradiating light, and can help to mitigate the inherent mismatch between photon absorption length and electron diffusion length in Cu_2O. In comparison to other works based on bare Cu_2O photocathodes on Cu substrates, our samples show excellent improvement on the photocurrent as well as the dark current. Thin and homogeneous Cu_2O layers obtained from the short deposition time (5 min) lead to the highest photocurrents, which is in agreement with the higher doping level that was observed by Mott-Schottky analysis. The UV–Vis transmission spectroscopy measurement also reveals that the free-standing porous Cu_2O has a transmittance of 23% which makes these structures promising candidates to be used in a tandem system with a photoanode in full PEC cells.

Acknowledgements

Mario Kurniawan is grateful for the financial support provided by the "Thüringer Graduiertenförderung" and the "TU Ilmenau Stipendium".

Funding

Open Access funding enabled and organized by Projekt DEAL.

Supplementary Information: The online version contains supplementary material available at https://doi.org/10.1007/s10853-021-06058-y.

References

[1] Glenk G, Reichelstein S (2019) Economics of converting renewable power to hydrogen. Nat Energy 4:216–222. https://doi.org/10.1038/s41560-019-0326-1

[2] Hisatomi T, Kubota J, Domen K (2014) Recent advances in semiconductors for photocatalytic and photoelectrochemical water splitting. Chem Soc Rev 43:7520–7535. https://doi.org/10.1039/c3cs60378d

[3] Walter MG, Warren EL, McKone JR et al (2010) Solar water splitting cells. Chem Rev 110:6446–6473. https://doi.org/10.1021/cr1002326

[4] Grätzel M (2001) Photoelectrochemical cells. Nature 414:338–344. https://doi.org/10.1038/35104607

[5] Golden TD, Shumsky MG, Zhou Y et al (1996) Electrochemical deposition of Copper(I) Oxide films. Chem Mater 8:2499–2504. https://doi.org/10.1021/cm9602095

[6] Rakhshani AE, Varghese J (1988) Potentiostatic electrodeposition of cuprous oxide. Thin Solid Films 157:87–96. https://doi.org/10.1016/0040-6090(88)90349-5

[7] Rakhshani AE, Al-Jassar AA, Varghese J (1987) Electrodeposition and characterization of cuprous oxide. Thin Solid Films 148:191–201. https://doi.org/10.1016/0040-6090(87)90157-X

[8] Ma X, Zhang J, Wang B et al (2018) Hierarchical Cu2O foam/g-C3N4 photocathode for photoelectrochemical hydrogen production. Appl Surf Sci 427:907–916. https://doi.org/10.1016/j.apsusc.2017.09.075

[9] Gerischer H (1977) On the stability of semiconductor electrodes against photodecomposition. J Electroanal Chem 82:133–143

[10] Zhang Y, Deng B, Zhang T et al (2010) Shape effects of Cu2O polyhedral microcrystals on photocatalytic activity. J Phys Chem C 114:5073–5079. https://doi.org/10.1021/jp9110037

[11] Tolstova Y, Wilson SS, Atwater HA (2015) Single phase, single orientation Cu2O (100) and (110) thin films grown by plasma-assisted molecular beam epitaxy. J Cryst Growth 410:77–81. https://doi.org/10.1016/j.jcrysgro.2014.10.045

[12] Chen A, Long H, Li X et al (2009) Controlled growth and characteristics of single-phase Cu 2 O and CuO films by pulsed laser deposition. Vacuum 83:927–930. https://doi.org/10.1016/j.vacuum.2008.10.003

[13] Akimoto K, Ishizuka S, Yanagita M et al (2006) Thin film deposition of Cu2O and application for solar cells. Sol Energy 80:715–722. https://doi.org/10.1016/j.solener.2005.10.012

[14] Paracchino A, Laporte V, Sivula K et al (2011) Highly active oxide photocathode for photoelectrochemical water reduction. Nat Mater 10:456–461. https://doi.org/10.1038/nmat3017

[15] Nitopi S, Bertheussen E, Scott SB et al (2019) Progress and perspectives of electrochemical CO2 reduction on copper in aqueous electrolyte. Chem Rev 119:7610–7672. https://doi.org/10.1021/acs.chemrev.8b00705

[16] An X, Li K, Tang J (2014) Cu2O/reduced graphene oxide composites for the photocatalytic conversion of CO2. Chemsuschem 7:1086–1093. https://doi.org/10.1002/cssc.201301194

[17] Paracchino A, Mathews N, Hisatomi T et al (2012) Ultrathin films on copper(i) oxide water splitting photocathodes: a study on performance and stability. Energy Environ Sci 5:8673. https://doi.org/10.1039/c2ee22063f

[18] Brittman S, Yoo Y, Dasgupta NP et al (2014) Epitaxially aligned cuprous oxide nanowires for all-oxide, single-wire solar cells. Nano Lett 14:4665–4670. https://doi.org/10.1021/nl501750h

[19] Lin CY, Lai YH, Mersch D, Reisner E (2012) Cu 2ONiO x nanocomposite as an inexpensive photocathode in photoelectrochemical water splitting. Chem Sci 3:3482–3487. https://doi.org/10.1039/c2sc20874a

[20] Wu H, Zheng Z, Toe CY et al (2020) A pulse electrodeposited amorphous tunnel layer stabilises Cu2O for efficient photoelectrochemical water splitting under visible-light irradiation. J Mater Chem A 8:5638–5646. https://doi.org/10.1039/d0ta00629g

[21] Azevedo J, Steier L, Dias P et al (2014) On the stability enhancement of cuprous oxide water splitting photocathodes by low temperature steam annealing. Energy Environ Sci 7:4044–4052. https://doi.org/10.1039/c4ee02160f

[22] Luo J, Steier L, Son MK et al (2016) Cu2O nanowire photocathodes for efficient and durable solar water splitting. Nano Lett 16:1848–1857. https://doi.org/10.1021/acs.nanolett.5b04929

[23] de Jongh PE, Vanmaekelbergh D, Kelly JJ (2000) Photoelectrochemistry of electrodeposited Cu[sub 2]O. J Electrochem Soc 147:486. https://doi.org/10.1149/1.1393221

[24] Engel CJ, Polson TA, Spado JR et al (2008) Photoelectrochemistry of porous p-Cu2 O films. J Electrochem Soc 155:37–42. https://doi.org/10.1149/1.2830850

[25] Jaeho Oh, Yongsug T, Jaeyoung L (2004) Electrodeposition of Cu2O nanowires using nanoporous alumina template. Electrochem Solid-State Lett 7:C27–C30. https://doi.org/10.1117/1.1640637

[26] Zhang W, Wen X, Yang S et al (2003) Single-crystalline scroll-type nanotube arrays of copper hydroxide synthesized at room temperature. Adv Mater 15:822–825. https://doi.org/10.1002/adma.200304840

[27] Wen X, Xie Y, Choi CL et al (2005) Copper-based nanowire materials: templated syntheses, characterizations, and applications. Langmuir 21:4729–4737. https://doi.org/10.1021/la050038v

[28] Paracchino A, Brauer JC, Moser JE et al (2012) Synthesis and characterization of high-photoactivity electrodeposited Cu 2O solar absorber by photoelectrochemistry and ultrafast

spectroscopy. J Phys Chem C 116:7341–7350. https://doi.org/10.1021/jp301176y

[29] Ahn CY, Lim MS, Hwang W et al (2017) Effect of porous metal flow field in polymer electrolyte membrane fuel cell under pressurized condition. Fuel Cells 17:652–661. https://doi.org/10.1002/fuce.201700042

[30] Varzi A, Mattarozzi L, Cattarin S et al (2018) 3D Porous Cu–Zn alloys as alternative anode materials for Li-ion batteries with superior low T performance. Adv Energy Mater 8:1–11. https://doi.org/10.1002/aenm.201701706

[31] Hao M, Charbonneau V, Fomena NN et al (2019) Hydrogen bubble templating of fractal Ni catalysts for water oxidation in alkaline media. ACS Appl Energy Mater 2:5734–5743. https://doi.org/10.1021/acsaem.9b00860

[32] Chaturvedi P, Sarker S, Chen X et al (2019) Enhancing the cooperative catalytic effect in Ni/Co Hydr(oxy)oxide porous electrodes for overall water splitting and glucose sensing. ACS Sustain Chem Eng 7:11303–11312. https://doi.org/10.1021/acssuschemeng.9b00822

[33] Shin HC, Liu M (2004) Copper foam structures with highly porous nanostructured walls. Chem Mater 16:5460–5464. https://doi.org/10.1021/cm048887b

[34] Still ER, Wikberg P (1980) Solution studies of systems with polynuclear complex formation. 1. The copper(II) citrate system. Inorganica Chim Acta 46:147–152. https://doi.org/10.1016/S0020-1693(00)84183-3

[35] Eskhult J, Nyholm L (2008) Pulsed galvanostatic and potentiostatic electrodeposition of Cu and Cu 2O nanolayers from alkaline Cu(II)-citrate solutions. J Electrochem Soc 155:2–9. https://doi.org/10.1149/1.2806793

[36] Yoon S, Kim M, Kim IS et al (2014) Manipulation of cuprous oxide surfaces for improving their photocatalytic activity. J Mater Chem A 2:11621–11627. https://doi.org/10.1039/c4ta00616j

[37] Cao D, Nasori N, Wang Z et al (2016) Facile surface treatment on Cu2O photocathodes for enhancing the photoelectrochemical response. Appl Catal B Environ 198:398–403. https://doi.org/10.1016/j.apcatb.2016.06.010

[38] Pourbaix M (1974) Atlas of electrochemical equilibria in aqueous solutions. National Association of Corrosion Engineers

[39] Wang JP, Cho WD (2009) Oxidation behavior of pure copper in oxygen and/or water vapor at intermediate temperature. ISIJ Int 49:1926–1931. https://doi.org/10.2355/isijinternational.49.1926

[40] Chen K, Xue D (2014) Reaction route to the crystallization of copper oxides. Appl Sci Converg Technol 23:14–26. https://doi.org/10.5757/asct.2014.23.1.14

[41] Yang Y, Xu D, Wu Q, Diao P (2016) Cu2O/CuO bilayered composite as a high-efficiency photocathode for photoelectrochemical hydrogen evolution reaction. Sci Rep 6:1–13. https://doi.org/10.1038/srep35158

[42] Plowman BJ, Jones LA, Bhargava SK (2015) Building with bubbles: the formation of high surface area honeycomb-like films via hydrogen bubble templated electrodeposition. Chem Commun 51:4331–4346. https://doi.org/10.1039/c4cc06638c

[43] Wang M, Yu X, Wang Z et al (2017) Hierarchically 3D porous films electrochemically constructed on gas-liquid-solid three-phase interface for energy application. J Mater Chem A 5:9488–9513. https://doi.org/10.1039/c7ta02519j

[44] Niu W, Moehl T, Cui W et al (2018) Extended Light Harvesting with Dual Cu2O-Based Photocathodes for High Efficiency Water Splitting. Adv Energy Mater 8. https://doi.org/10.1002/aenm.201702323

[45] Ma QB, Hofmann JP, Litke A, Hensen EJM (2015) Cu2O photoelectrodes for solar water splitting: tuning photoelectrochemical performance by controlled faceting. Sol Energy Mater Sol Cells 141:178–186. https://doi.org/10.1016/j.solmat.2015.05.025

[46] Bai J, Li Y, Wang R et al (2015) A novel 3D ZnO/Cu2O nanowire photocathode material with highly efficient photoelectrocatalytic performance. J Mater Chem A 3:22996–23002. https://doi.org/10.1039/c5ta07583a

[47] Huang Q, Kang F, Liu H et al (2013) Highly aligned Cu2O/CuO/TiO2 core/shell nanowire arrays as photocathodes for water photoelectrolysis. J Mater Chem A 1:2418–2425. https://doi.org/10.1039/c2ta00918h